J. Appl. Comput. Mech., 8(2) (2022) 617-628
DOI: 10.22055/JACM.2021.38664.3264

ISSN: 2383-4536
jacm.scu.ac.ir

Shahid Chamran University of Ahvaz

Journal of Applied and Computational Mechanics

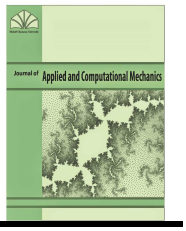

Research Paper

A Stress Tensor-based Failure Criterion for Ordinary State-based Peridynamic Models

Daniele Dipasquale[1], Giulia Sarego[2], Prasert Prapamonthon[3], Soemsak Yooyen[4], Arman Shojaei[5]

[1] Department of Aeronautical Engineering, International Academy of Aviation Industry, King Mongkut's institute of Technology Ladkrabang, Bangkok 10520, Thailand, Email: daniele.di@kmitl.ac.th

[2] Department of Industrial Engineering, University of Padova, Via Venezia 1, Padova 35131, Italy, Email: giulia.sarego@gmail.com

[3] Department of Aeronautical Engineering, International Academy of Aviation Industry, King Mongkut's institute of Technology Ladkrabang, Bangkok 10520, Thailand, Email: prasert.pr@kmitl.ac.th

[4] Department of Aeronautical Engineering, International Academy of Aviation Industry, King Mongkut's institute of Technology Ladkrabang, Bangkok 10520, Thailand, Email: soemsak.yo@kmitl.ac.th

[5] Institute of Material Systems Modeling, Helmholtz-Zentrum Hereon, Max-Planck-Str. 1, 21502 Geesthacht, Germany, Email: arman.shojaei@hereon.de

Received September 23 2021; Revised November 30 2021; Accepted for publication December 10 2021.
Corresponding author: A. Shojaie (arman.shojaei@hereon.de)

Abstract. Peridynamics is a recent nonlocal theory of continuum mechanics that is suitable to describe fracture problems in solid mechanics. In this paper, a new failure criterion based on the stress field is developed by adopting the damage correspondence model in the ordinary state-based peridynamic theory. The proposed stress tensor-based failure criterion is capable of predicting more accurately crack propagation in the mixed mode I-II fracture problems different from other failure criteria in peridynamics. The effectiveness of the proposed model is demonstrated by performing several examples of mixed-mode dynamic fracture in brittle materials.

Keywords: State-based peridynamics; fracture criteria; dynamic crack propagation; mixed-mode loading.

1. Introduction

Predicting the failure of a component in consequence of the nucleation and propagation of cracks is still a challenging problem for the computational mechanics community [1-3]. Numerous theories and numerical methods have been developed in the last decades in order to capture the complex phenomena that control the driving force of the crack nucleation and propagation [4-9]. Numerical methods based on the classical theory of mechanics, such as the eXended Finite Element Method (XFEM) [10], circumvent the problem related to the undefined spatial derivatives in the proximity of discontinuities by means of ad hoc auxiliary equations to decide how the crack propagates in the medium. Such auxiliary equations become cumbersome especially in 3D analysis characterized by complex crack patterns. Other strategies for studying the crack propagation adopt interface elements and Cohesive Zone Models (CZM) [11-13] which can be mainly applied if the region where the crack path should appear is known a priori. Moreover, the crack path may be strongly sensitive to the type of adopted discretization. Recently, the Phase-Field method [14] has shown a great potential in treating discontinuities such as fracture and damage, but it has some limitations such as the nucleation is based on strain energy density and not on stress tensor, spurious branching formation and inconsistency of branching patterns are observed with respect to the ones observed in experiments. However, differently from all the other theories, peridynamics (PD), a new nonlocal theory of continuum developed by Silling and Silling et al. [15, 16] is capable of treating the fracture with extreme simplicity [17-34]. PD is classified as nonlocal since the governing equation of motion is defined by assuming that any material point of a body can interact with each other if their distance is within a certain length called horizon. This length can be related to the length scale of the material as well as the phenomenon studied [35-37]. In PD, crack nucleation and propagation in a medium is commonly introduced by removing the interaction between the material points (called bond) if the stretch of the bond is above a certain stretch whose value is related to the fracture energy of the material in mode I [17]. This critical stretch-based failure criterion is mainly introduced for studying the crack propagation in mode I of fracture. Indeed, although bonds can break under shear deformation, the criterion neglects the contribution of deviatoric part of the deformation energy to the total elastic energy stored in the bond. In order to overcome this shortcoming, another criterion based on the energy stored in a bond is proposed in [38], while a similar energy-based failure criterion is employed in [39] including the J-integral computation in the proximity of the crack tip. However, both criteria have been tested only by performing

Published online: December 10 2021

simulations under mode I loading. More complex failure criteria such as the equivalent strain criterion presented in [40] and the standard Johnson-Cook damage model presented in [41] have been applied by adopting the correspondence material model introduced by Silling [42]. According to this model, the material model from the local theory of mechanics is combined with the nonlocal capabilities of PD. According to the correspondence material model, the classical failure criteria adopted in the classical theory of mechanics can be used for deciding when a bond should be broken. In this way, both deviatoric and volumetric strains during the fracture process are taken into account to make the model more suitable for studying the crack propagation under mixed-mode I-II loading.

So far, to the authors' knowledge, no studies have been carried out in order to apply the correspondence material models introduced in [42] for studying the dynamic mixed-mode I-II fracture in brittle materials. Therefore, this work aims to develop a new failure criterion for PD which is based on the use of a failure criterion commonly adopted in the classical mechanics, such as the Maximum Normal Stress Criterion (MNSC) mainly used to predict the failure in brittle materials in the framework of the classical theory of mechanics. In order to achieve this goal, the classical MNSC has to be adapt to the nonlocal nature of PD. By doing so, substantial advantages can be obtained thanks to the reliable results given by the classical failure criteria and the ease of peridynamic formulation to simulate the crack propagation. We remark that with the proposed method other failure criteria such as Tresca and Mises criteria might be employed, the choice of using the MNSC is based on the fact that the dynamic crack propagation in brittle materials is simulated in this work. After an overview of the state-based peridynamic theory given in Sect. 2, we introduce the new failure criterion based on the classic stress tensor which takes inspiration from the approach proposed by [16] in Sect. 3. Then in Sect. 4, we simulate some benchmark problems of dynamic crack propagation of mixed I-II fracture to validate our criterion. Finally, the conclusions are highlighted in Sect. 6. It should be remarked here that the interested reader may refer to [16] for more details on the mathematical operations used in state-based PD.

2. Overview of Ordinary State-based Peridynamics

The integro-differential equation of motion defined by PD [37] can be expressed at each material point $\mathbf{x}$ of a body at the instant of time t as

$$\rho(\mathbf{x})\ddot{\mathbf{y}}(\mathbf{x},t)=\int_{H_{\mathbf{x}}}\left[\underline{\mathbf{T}}[\mathbf{x},t]\langle\mathbf{p}-\mathbf{x}\rangle-\underline{\mathbf{T}}[\mathbf{p},t]\langle\mathbf{x}-\mathbf{p}\rangle\right]\mathrm{dV}_{\mathbf{p}}+\mathbf{b}(\mathbf{x},t) \tag{1}$$

where ρ is the mass density, $\mathbf{y}$ is the current position vector of the material point, $\ddot{\mathbf{y}}$ is the acceleration vector of point $\mathbf{x}$, $\underline{\mathbf{T}}[\mathbf{x},t]\langle\mathbf{p}-\mathbf{x}\rangle$ is the force state associated with the bond $\boldsymbol{\xi}$ = $\mathbf{p}$ - $\mathbf{x}$ and applied to point $\mathbf{x}$ (called the source point), $\mathrm{dV_P}$ is the infinitesimal volume associated to point $\mathbf{p}$ (called the family point), H_x is the neighborhood of $\mathbf{x}$ (a circle in 2D domains centered at the source point with radius δ called horizon) and $\mathbf{b}$ is the body vector forces. Let us define the following PD variables such as the reference position state $\underline{\mathbf{X}}$, the displacement state $\underline{\mathbf{Y}}$ and the deformation state $\underline{\mathbf{U}}$ as

$$\begin{aligned}\underline{\mathbf{X}}\langle\mathbf{p}-\mathbf{x}\rangle&=\mathbf{p}-\mathbf{x}\\ \underline{\mathbf{U}}\langle\mathbf{p}-\mathbf{x}\rangle&=\mathbf{u}(\mathbf{p},t)-\mathbf{u}(\mathbf{x},t)\\ \underline{\mathbf{Y}}\langle\mathbf{p}-\mathbf{x}\rangle&=\underline{\mathbf{X}}\langle\mathbf{p}-\mathbf{x}\rangle+\underline{\mathbf{U}}\langle\mathbf{p}-\mathbf{x}\rangle\end{aligned} \tag{2}$$

Assuming the constitutive model called Linear Peridynamic Solid (LPS), introduced in [41], the force state of the ordinary state-based PD for plane stress problems can be expressed by [40]

$$\underline{\mathbf{T}}[\mathbf{x},t]\langle\mathbf{p}-\mathbf{x}\rangle=\left\{\frac{2(2\upsilon-1)}{\upsilon-1}\left[\left(K+\frac{\mu}{9}\frac{(\upsilon+1)^2}{(2\upsilon-1)^2}\right)\theta-\frac{8\mu}{3q}\left(\underline{\omega e^d}\right)\bullet\underline{x}\right]\underline{\underline{\omega x}}+\frac{8\mu}{q}\underline{\omega e^d}\right\}\cdot\frac{\underline{\mathbf{Y}}\langle\mathbf{p}-\mathbf{x}\rangle}{\underline{\mathbf{Y}}\langle\mathbf{p}-\mathbf{x}\rangle} \tag{3}$$

where θ stands for the PD scalar-valued function dilatation function computed for plane stress condition in [43] as

$$\theta=\frac{2(2\upsilon-1)}{(\upsilon-1)}\frac{\underline{\omega x}\bullet\underline{e}}{q} \tag{4}$$

in which ω demotes the influence function (i.e., the weight of the single bond in the overall computation), $\underline{x}$ represents the reference position scalar state (which maps a bond to its undeformed length in the initial configuration), $\underline{e}=\|\underline{\mathbf{Y}}\|-\|\underline{\mathbf{X}}\|$ is the scalar extension (elongation) state and q is the weighted volume/area of the neighborhood (horizon region) in 2D defined by

$$q=\int_{H_{\mathbf{x}}}\underline{\omega x}.\underline{x}\mathrm{dV} \tag{5}$$

$\underline{e}^d=\underline{e}-\theta\|\underline{\mathbf{X}}\|/3$ stands for the scalar deviatoric state component of the bond elongation, K is the bulk modulus, μ is the shear modulus and ν is Poisson's ratio. The local damage, interpreted as local degradation of the mechanical behavior, can be defined uniquely at every point by breaking irreversibly the bonds connecting to the family points when a failure criterion is met (i.e., $s > s_0$). The criterion, commonly adopted by the PD community, is based on the concept of the critical stretch s_0, where the stretch of a bond s is defined as

$$s=\frac{\underline{e}\langle\mathbf{p}-\mathbf{x}\rangle}{\|\underline{\mathbf{X}}\langle\mathbf{p}-\mathbf{x}\rangle\|} \tag{6}$$

The critical stretch is derived from the fracture energy of the material G_0 in mode I [17], hence the bond breaks when its stretch is higher than the critical stretch. Noting that such a failure criterion neglects completely the contribution of the deviatoric part of the deformation to the total stored elastic energy in the bond. Indeed, this criterion is originally introduced in bond-based PD formulation [17] for dealing with mode I brittle fracture problems. At this point, the damage at the material point $\mathbf{x}$ can be computed as

$$\varphi(\mathbf{x},t)=1-\frac{\int_{H_\mathbf{x}}\lambda(\mathbf{p}-\mathbf{x},t)\mathrm{dV_p}}{\int_{H_\mathbf{x}}\mathrm{dV_p}} \tag{7}$$

where λ is a scalar-valued function which assumes the value 1 if the bond is active and 0 if the bond is broken. $\varphi=0$ means the undamaged state, while $\varphi=1$ implies the complete separation of the source point of all the family points. The most common method to implement a PD model numerically is based on a strong-form meshfree scheme [17]. In this way, the whole domain is discretized through a uniform grid of nodes with grid spacing $\Delta x = \Delta y$ for 2D analyses. A spatial one-point Gauss quadrature is adopted so that each node $\mathbf{x}_i$ is located at the center of its assigned volume $V_i = (\Delta x)^2\, t_b$, being t_b the thickness of the analyzed body. Therefore, (1) can be rewritten in the discrete form as

$$\rho_i\ddot{\mathbf{y}}_i^n=\sum_{j\in\mathcal{F}_i}\left\{\underline{\mathbf{T}}\left[\mathbf{x}_i^n\right]\langle\mathbf{x}_j^n-\mathbf{x}_i^n\rangle-\underline{\mathbf{T}}\left[\mathbf{x}_j^n\right]\langle\mathbf{x}_i^n-\mathbf{x}_j^n\rangle\right\}\beta_j V_j+\mathbf{b}_i^n \tag{8}$$

where the summation runs over the list of family nodes $\mathcal{F}_i$ within the neighborhood of $\mathbf{x}_i$, n stands for the considered time step and β_j, called the volume correction factor, is introduced for computing the portion of the volume of the family node $\mathbf{x}_j$ covered by the neighborhood $H_{\mathbf{x}_i}$. In this work, the volume correction factor is calculated according to the algorithm adopted in [44]. (8) is solved in time making use of the explicit Velocity-Verlet scheme:

$$\begin{aligned}\dot{\mathbf{y}}^{n+\frac{1}{2}}&=\dot{\mathbf{y}}^n+\frac{\Delta t}{2}\ddot{\mathbf{y}}^n\\ \mathbf{y}^{n+1}&=\mathbf{y}^n+\Delta t\dot{\mathbf{y}}^{n+\frac{1}{2}}\\ \dot{\mathbf{y}}^{n+1}&=\dot{\mathbf{y}}^{n+\frac{1}{2}}+\frac{\Delta t}{2}\ddot{\mathbf{y}}^{n+1}\end{aligned} \tag{9}$$

where the constant time step Δt is commonly chosen to be smaller than the critical time step $\Delta t_c = \Delta x/c_l$, with c_l the speed of the longitudinal wave in the medium. The accuracy of the numerical solution is governed by two parameters such as the horizon δ and the $m=\delta/\Delta x$ ratio [45].

3. The Proposed Failure Criterion

The criterion presented in the following is based on the stress field tensor and takes inspiration from the approach proposed in [40]. According to the correspondence model introduced by Silling [42], which allows to adopt in state-based PD theory, the constitutive material models described in terms of the stress tensor of the classical theory, a nonlocal approximation of the deformation gradient tensor can be represented by means of the following expression

$$\overline{\mathbf{F}}=\left(\int_{H_\mathbf{x}}\underline{\omega}\langle\mathbf{p}-\mathbf{x}\rangle\underline{\mathbf{Y}}\langle\mathbf{p}-\mathbf{x}\rangle\otimes(\mathbf{p}-\mathbf{x})\mathrm{dV_p}\right)\mathbf{K}^{-1} \tag{10}$$

where $\mathbf{K}$ is the symmetric positive definite shape tensor defined as

$$\mathbf{K}=\int_{H_\mathbf{x}}\underline{\omega}\langle\mathbf{p}-\mathbf{x}\rangle(\mathbf{p}-\mathbf{x})\otimes(\mathbf{p}-\mathbf{x})\mathrm{dV_p} \tag{11}$$

Consequently, Piola stress tensor $\overline{\boldsymbol{\sigma}}$ can be expressed as

$$\overline{\boldsymbol{\sigma}}=\hat{\sigma}\left(\overline{\mathbf{F}}\right) \tag{12}$$

where $\hat{\sigma}$ represents a general function between the stress and the strain tensor. In this work, due to the assumption that the material is linearly elastic and isotropic, the stress and strain components are related through the well-known Hooke's constitutive law as

$$\begin{bmatrix}\sigma_{xx}\\ \sigma_{yy}\\ \sigma_{xy}\end{bmatrix}=\begin{bmatrix}K+\mu & K-\mu & 0\\ K-\mu & K+\mu & 0\\ 0 & 0 & \mu\end{bmatrix}\begin{bmatrix}\dfrac{\partial u}{\partial x}\\ \dfrac{\partial v}{\partial y}\\ \dfrac{1}{2}\left(\dfrac{\partial u}{\partial y}+\dfrac{\partial v}{\partial x}\right)\end{bmatrix} \tag{13}$$

with u and v the displacements along x and y reference system, respectively. Therefore, (8)-(11) allow to determine the state of stress (see Fig. 1a) at each node of the domain regardless of the presence of cracks in the specimen. The idea proposed by this criterion is based on the assumption that a node of the grid is identified as a *potential candidate* for introducing the fracture when the tension at that point reaches a critical tension according to the failure criteria adopted by the classical theory of mechanics.

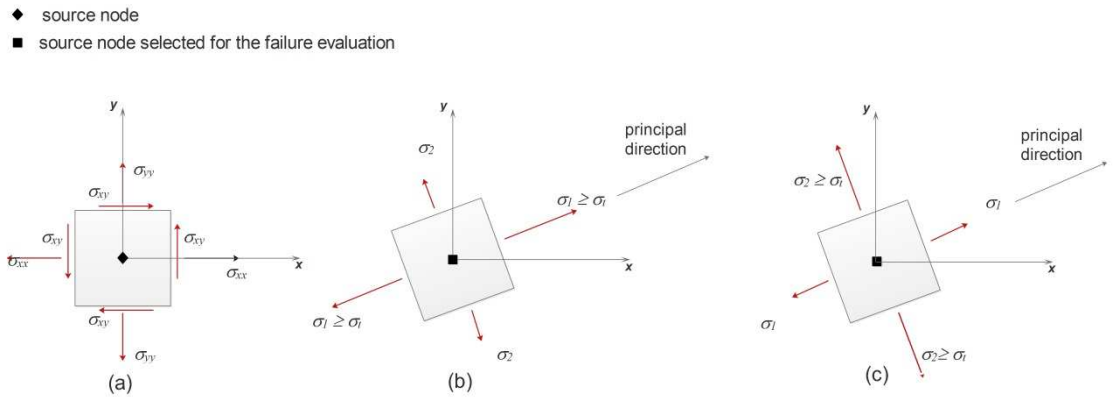

Fig. 1. The strategy for choosing the source node as "potential" failure node: (a) calculation of the stress tensor at the source node, (b) the source node is selected if $\sigma_1 \geq \sigma_t$, (c) the source node is selected if $\sigma_2 \geq \sigma_t$.

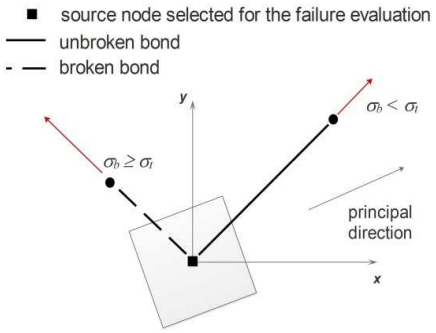

Fig. 2. Strategy adopted for breaking a bond.

We highlight the term "potential" to remark that, differently from the classical theory of mechanics, PD deals with bonds. Let us give insight into the criterion proposed in this work. To begin with, we employ the criterion named Maximum Normal Stress Criterion (MNSC) commonly used to predict the failure of brittle materials. According to MNSC, a node $\mathbf{x}$ will be marked as *failed* if its maximum principal stress exceeds the uniaxial tensile strength σ_t of the material. Alternatively, the node will be marked as failed if the minimum principal stress is lower than the uniaxial compressive strength σ_c of the material. Fig. 1 shows the application of MNSC for the only case of tensile stress. If the criterion is satisfied, we evaluate the stress σ_b at the family node $\mathbf{p}$ along the direction of the bond $\boldsymbol{\xi} = \mathbf{p} - \mathbf{x}$, recalling the Cauchy's relation in matrix form, as

$$\begin{bmatrix} \sigma_{b,x} \\ \sigma_{b,y} \end{bmatrix} = \left(\frac{\sigma_x + \sigma_y}{2} + \frac{\sigma_x - \sigma_y}{2} \cos(2\alpha) + \sigma_{xy} \sin(2\alpha) \right) \begin{bmatrix} \cos(\alpha) \\ \sin(\alpha) \end{bmatrix} \tag{14}$$

where $\sigma_{b,x}$ and $\sigma_{b,y}$ are the corresponding components in the reference system (x,y); moreover, α denotes the angle between the bond and the x-axis evaluated at the family node. Therefore, the breakage of the bond will be activated if $\sigma_b \geq \sigma_t$ or if $\sigma_b \leq \sigma_c$. Fig. 2 shows the adopted approach for the case of tensile stress. The proposed approach might be also applied for non- uniform grids such as dual-horizon peridynamics [46-47] or in the context of other meshless methods [48]. Moreover, the proposed criterion is not limited to the 2D cases but it can be extended to 3D cases. We want to remark that although our method takes inspiration from the one developed in [40], the breakage of the bond is based on the use of two approaches which are completely different. Indeed, in [40] two methods are used in order to decide if a bond should be broken, the first one utilizes the equivalent strain which is a measure of the shearing strain and the second one considers the averaged value of the volumetric strain (dilatation) obtained for the principle directions which is given by the summation of the three strain invariants.

4. Numerical Results

The effectiveness of the proposed failure criterion to capture the mix-mode fracture is shown by simulating numerically three benchmark problems. The analyses are carried out by performing both the m-convergence and the δ-convergence so that the influence of the PD parameters on the simulated fracture paths is evaluated. For the former convergence, the horizon length is maintained constant increasing the number of nodes enclosed in it, while for the latter convergence, the number of nodes enclosed inside the horizon is kept constant reducing the horizon length. In-house codes are developed by means of the commercial software Matlab for the numerical implementation of the Ordinary State-Based theory. The computational time of the simulations carried out in the following is approximately in the range of 9-10 h for the most refined peridynamic grids. Moreover, for all cases treated the crack speed is always lower than the theoretical upper limit of crack speed (Rayleigh wave speed).

4.1 PMMA plate subjected to mixed-mode loads

The first benchmark problem concerns a square pre-cracked plate with size 2w = 150 mm, thickness t_b = 5 mm, and an initial crack of length 2a = 45 mm subjected to a static traction load by means of a universal tensile testing machine (see Fig. 3). The problem was experimentally performed in [49] and it consists of a specimen that is loaded diagonally by two opposite concentrated loads.

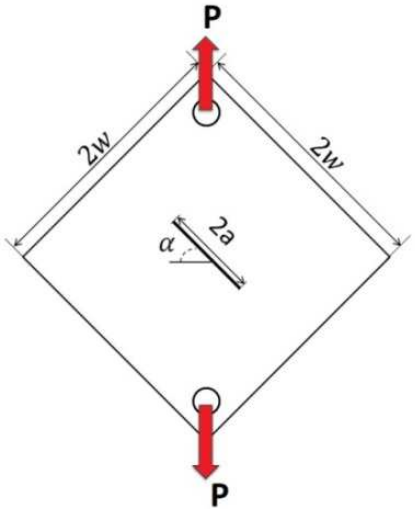

Fig. 3. The set-up: the square pre-cracked plate diagonally loaded [49].

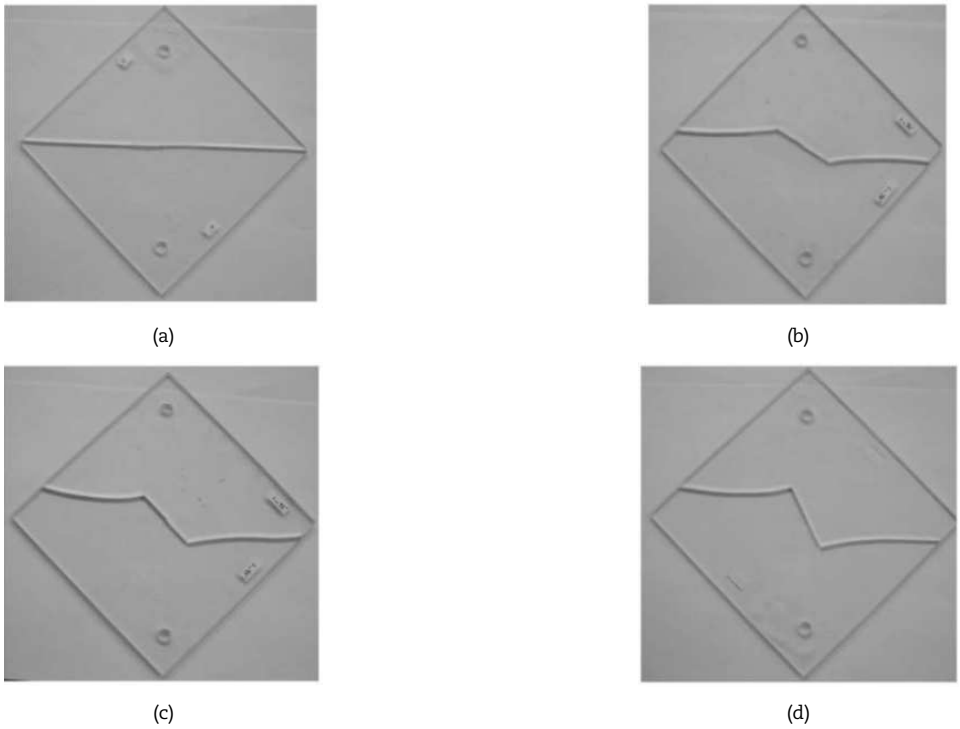

Fig. 4. The fracture paths observed in [49] of the specimen for different initial crack inclinations: (a) $\alpha = 0°$ (Pure mode I), (b) $\alpha = 30°$, (c) $\alpha = 45°$, (d) $\alpha = 62.5°$ (Pure mode II).

Varying the initial crack inclination α leads the crack to propagate from the pure mode I ($\alpha = 0°$) to the pure mode II ($\alpha = 62.5°$), while for inclinations enclosed inside that range the crack propagates under a mixed-mode I -II loading (see Fig. 4). The cases analysed in [48] and simulated in this work comprise the inclinations $\alpha = 0°, 30°, 45°, 62.5°$; the same benchmark problem was numerically studied in [50, 51] by applying the classical failure methods adopted by the PD community. The grid used for the simulation with the applied boundary conditions is displayed in Fig. 5. The results obtained for the δ-convergence and *m*-convergence are displayed in Fig. 6 and Fig. 7, respectively. Fig. 6 shows how the reduction of the horizon size leads the simulated cracks to be closer to the experimental crack patterns. This shows a good agreement with the experimental results when the horizon has a size equals to 4 mm, except for the case of the pure mode II in which the simulated crack propagates by deviating slightly from the experimental path. An improvement of the results is obtained by adopting the m-convergence (see Fig. 7); in particular, when the m-ratio is set to 4. However, a certain sensitivity to the PD parameters (horizon and m-ratio) on the results obtained with MNSC criterion may be observed, this mainly relies in the lack of data concerning the length-scale of the material involved in the specimen. Indeed, as stated in [36], the horizon should be selected according to the length-scale of the material which is related to its microstructure. Moreover, a m-ratio higher than 6 should be selected in order to reduce the dependence of crack propagation on orientation of regular grids, as shown in [52]. Finally, in Fig. 8, a comparison between the proposed failure criterion and that one based on the critical stretch is displayed, showing how the MNSC criterion is capable of predicting the mixed-mode loading (with reference to the cases $\alpha = 30°$ and $\alpha = 45°$) better than the critical stretch-based criterion. However, slight differences may be observed between the experimental paths and the simulated ones in consequence of the elastic waves generated by the dynamically applied load and also by the local imperfections of the real plates, when compared to the flawless simulated ones.

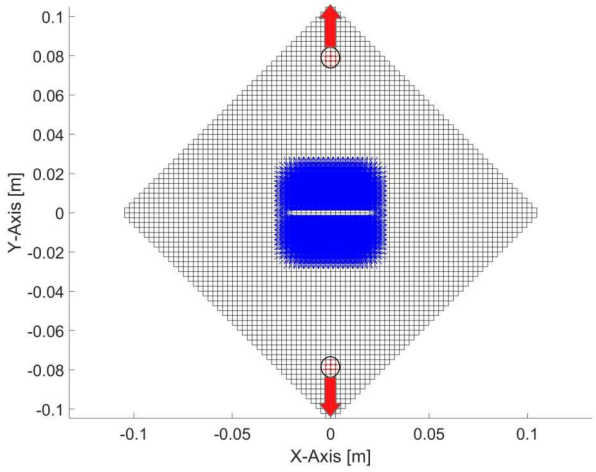

Fig. 5. PD grid with the applied boundary conditions and visualization of the network of bonds where the initial crack is introduced.

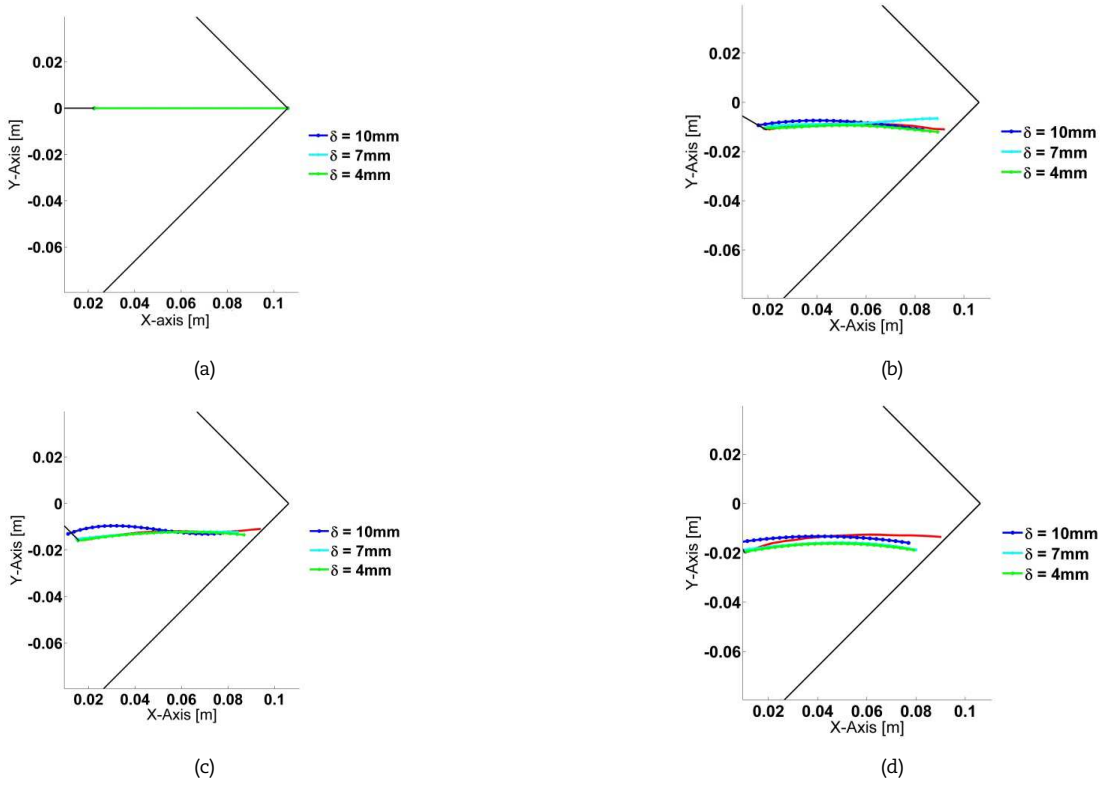

Fig. 6. The results for δ-convergence (*m*-ratio = 4) with MNSC criterion: (a) α = 0°, (b) α = 30°, (c) α = 45°, (d) α = 62.5°. The red line represents the experimental crack path.

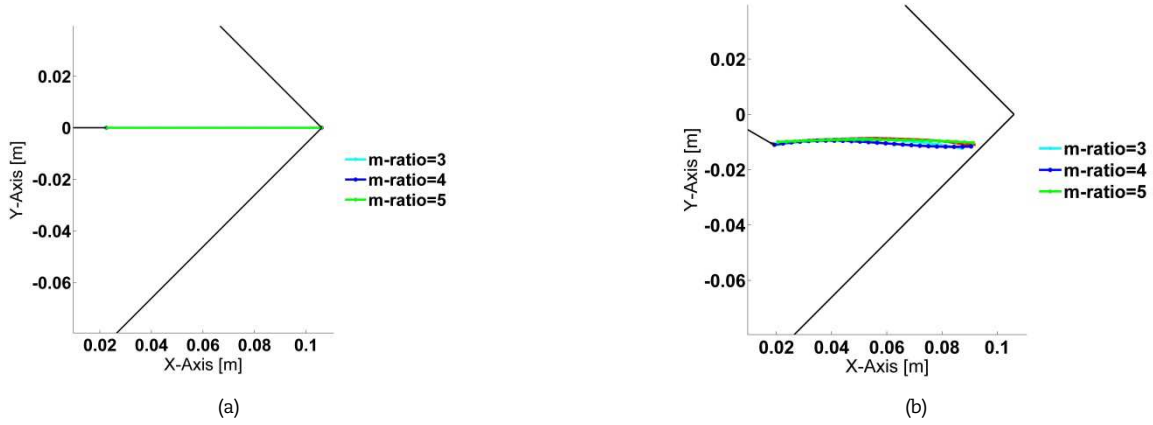

Fig. 7. The results for *m*-convergence (δ = 5 mm) with MNSC criterion: (a) α = 0°, (b) α = 30°, (c) α = 45°, (d) α = 62.5°. The red line represents the experimental crack path.

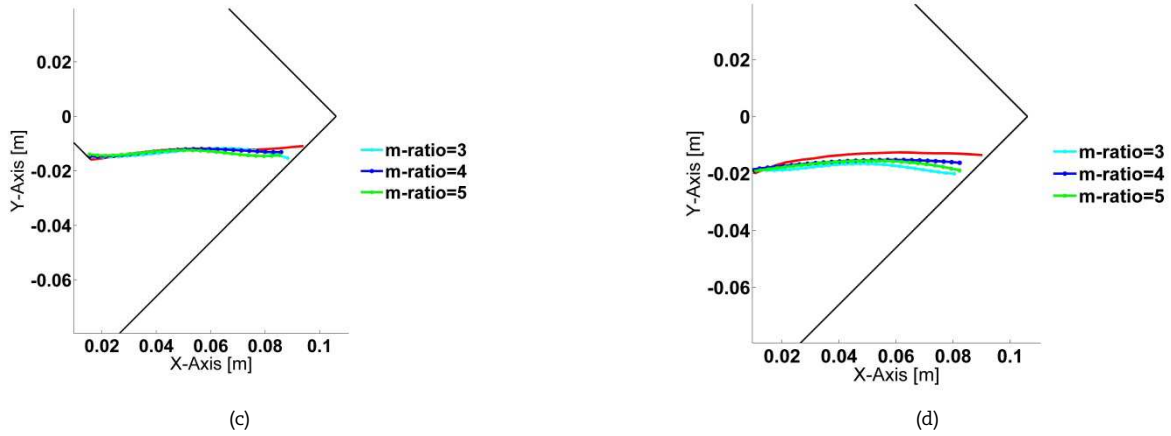

(c) (d)

Fig. 7. Continued.

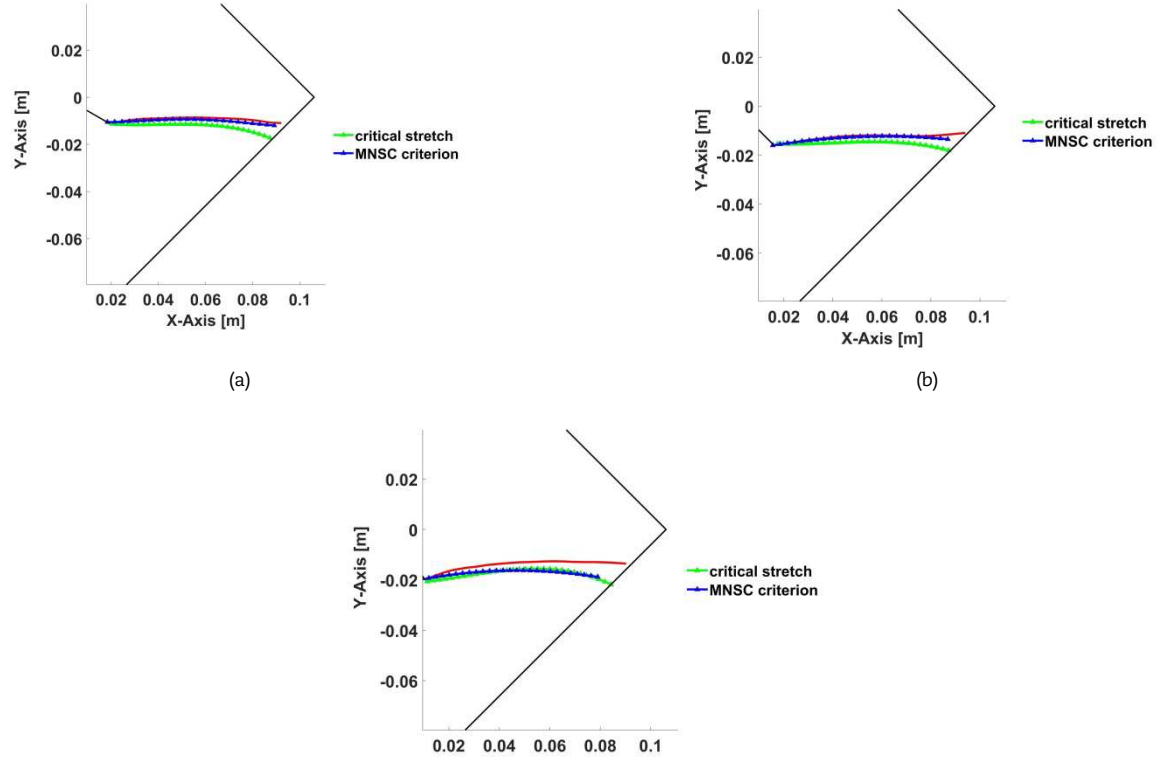

(a) (b)

(c)

Fig. 8. Comparison between MNSC and critical stretch criterion for the case of δ = 4 mm and m-ratio = 4: (a) α = 30°, (b) α = 45°, (c) α = 62.5°. The red line represents the experimental crack path.

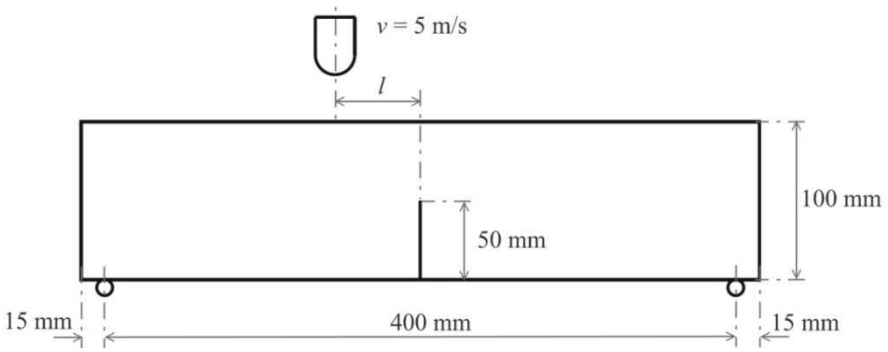

Fig. 9. The set-up of the loading condition for the three-points bending test [53].

4.2 Impact of a PMMA pre-notched beam

The second benchmark problem concerns a pre-notched beam subjected to an impact load tested experimentally in [53] and numerical simulations are carried out in [53, 54]. As shown in Fig. 9, a three-point bend specimen of length L = 430 mm, width W = 100 mm, thickness t_b = 10 mm and an initial crack of length 2a = 50 mm is hit by a hammer on the upper side of the specimen at the off-centre of its length. The loading eccentricity is defined as e = l/(L/2), as reported in [53], only the cases with a loading eccentricity of e = 0 and e = 0.1 are analyzed. Fig. 10 shows the snapshots of the crack patterns captured during the experiment performed in [53].

Both δ-convergence and *m*-convergence are carried out to evaluate the effects of the horizon size and the number of nodes enclosed within the horizon on the fracture path. An example of PD grid adopted for the analysis is shown in Fig. 11. A velocity of v = 5 m/s is imposed on few nodes of the upper side of the model (red circles shown in Fig. 11) and the roller support constraints are applied on the left and right lower side of the model as shown by the green triangles in Fig. 11. A critical time step of Δt_c = 300 ns is adopted to solve numerically the equation of motion (6) for the finest grid characterized by a grid spacing Δx = 0.6 mm, horizon δ = 3 mm and *m*-ratio = 5; moreover, a plane stress condition is assumed. The mechanical properties of the PMMA material are: Young's modulus E = 2.94 GPa, Poisson's ratio ν = 0.3, and mass density ρ = 1190 kg/m^3. Due to the lack of data given in [53], regarding the tensile strength of the specimens tested, a tensile strength σ_t = 5 MPa is chosen so that the crack for the case e = 0 starts propagating approximately at time 156 ms; see [53] for more details. In addition, as explained previously, the fracture is set to be activated by using only the tensile strength since brittle materials are weak in tension.

Fig. 12 shows the simulated crack paths at time t = 210 ms for the case e = 0.1, while for the case e = 0 no results are shown since all the simulations perfectly satisfy the symmetry of the treated problem (as shown in the previous benchmark problem). Interestingly, Fig. 12a indicates how the reduction of the horizon leads the simulated cracks to match better the experimental path; besides, the paths look to be slightly longer. This may be explained as a consequence of adopting the suggested value for the tensile strength of the material. However, Fig. 12b shows how the slope of the crack path obtained by the most refined grid is in good agreement with the experimental crack. Finally, Fig. 13 shows a comparison between the PD results obtained with the finest grid and other numerical results given in [53] and that one given by PD with the critical stretch-based failure criterion. This remark points out how the proposed stress criterion MNSC applied to PD is capable to capture almost accurately the experimental crack.

4.3 Impact of a pre-notched concrete beam

The last benchmark problem concerns the mixed mode fracture of a three point bending test where a beam made of concrete is impacted by a cylinder projector with initial velocity of 0.05 m/s at the center of its upper side [55], the set-up is shown in Fig. 14. In [55], three cases are studied experimentally and numerically depending on the different position of the notches with respect to the center of the beam. The same problem is studied numerically in [56]. In this work, only one case of mixed mode fracture is carried out in order to compare our stress-based failure criterion with the classic critical stretch. The material has the following mechanical properties: Young's modulus E = 29 GPa, Poisson's ratio ν = 0.2, mass density ρ = 2400 kg/m^3, fracture energy release rate G = 31.1 J/m^2 and tensile strength σ_t = 3 MPa. The grid has 45600 nodes with grid spacing Δx = 0.67 mm and *m*-ratio = 5, the model with the applied boundary conditions are shown in Fig. 15. A critical time step of Δtc = 150 ns is adopted to solve numerically the equation of motion (6) and the plane stress condition is considered.

(a) (b)

Fig. 10. High-speed photographs captured in [53] of the dynamically fracturing specimen: (a) e = 0, (b) e = 0.1.

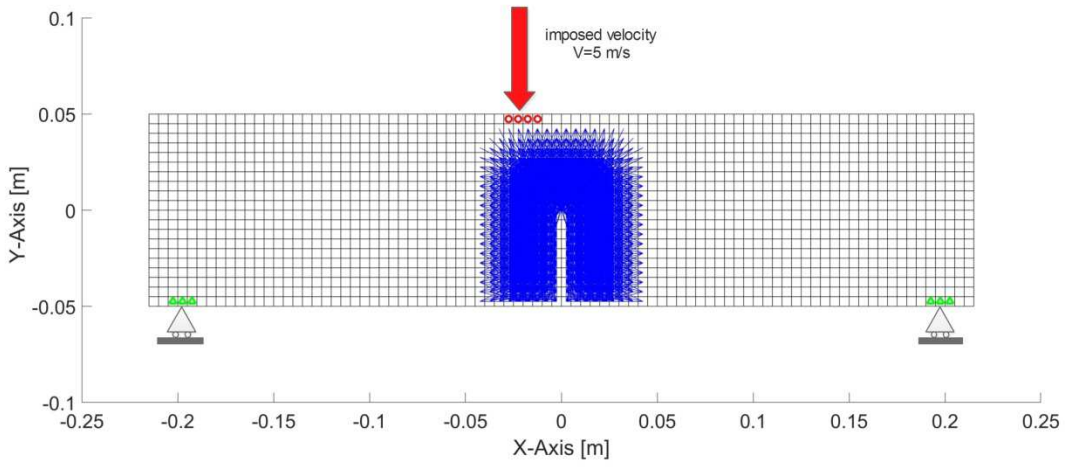

Fig. 11. The PD grid with the applied boundary conditions and visualization of the network of bonds where the initial crack is introduced.

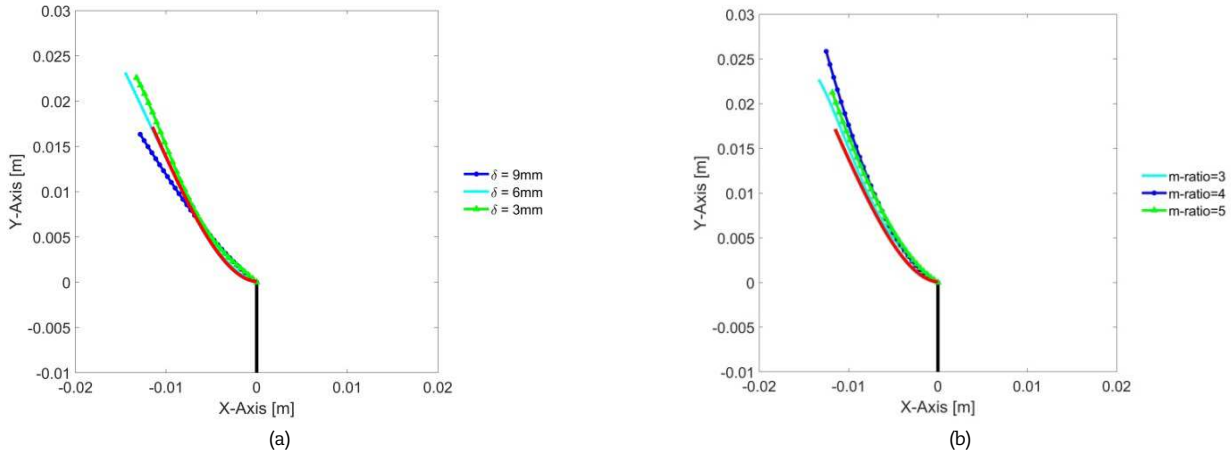

Fig. 12. Results for: (a) δ-convergence (*m*-ratio = 3), (b) *m*-convergence (δ = 3 mm). The red line represents the experimental crack pattern.

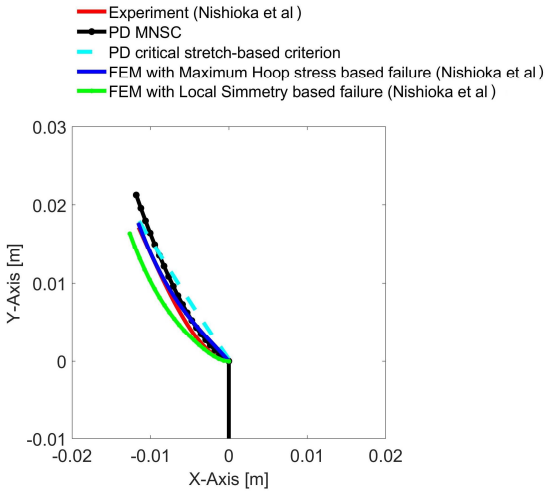

Fig. 13. Comparison between the PD results obtained with the most refined grid (δ = 3 mm, m = 5) and the results reported in [53] and the results obtained with PD by applying the critical stretch-based failure criterion.

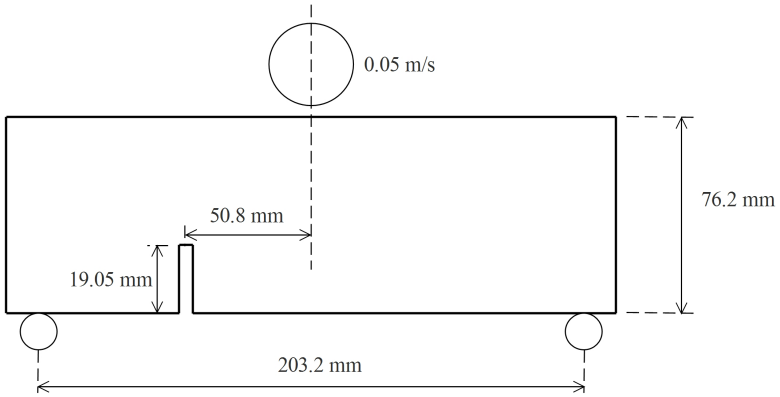

Fig. 14. Set-up of the three-point bending experiment [55].

The results obtained with the stress-based failure criterion and the critical stretch are shown in Fig. 16 and Fig. 17, respectively. It can be notice how the crack path obtained by using the stress-based failure criterion fits the experimental fracture patterns better than the one obtained by using the classic critical stretch. We can draw the conclusion that the proposed method is more suitable for capturing the mixed mode fracture.

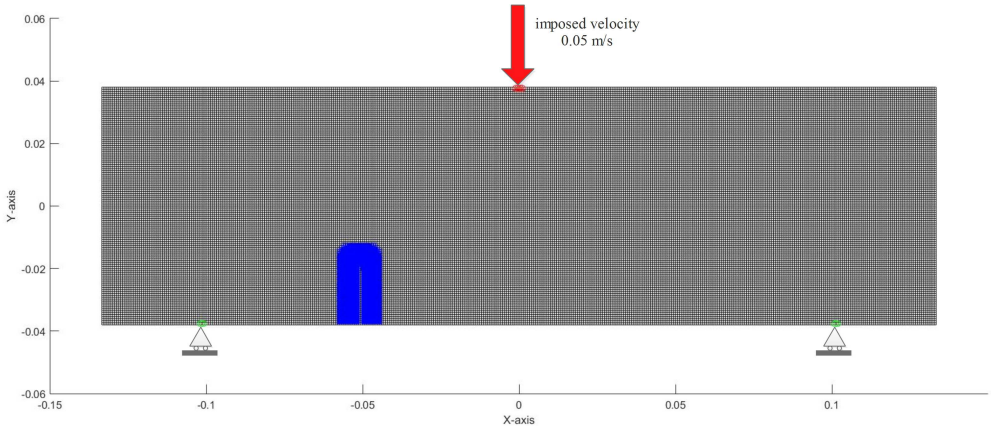

Fig. 15. The PD grid with the applied boundary conditions and visualization of the network of bonds where the initial crack is introduced.

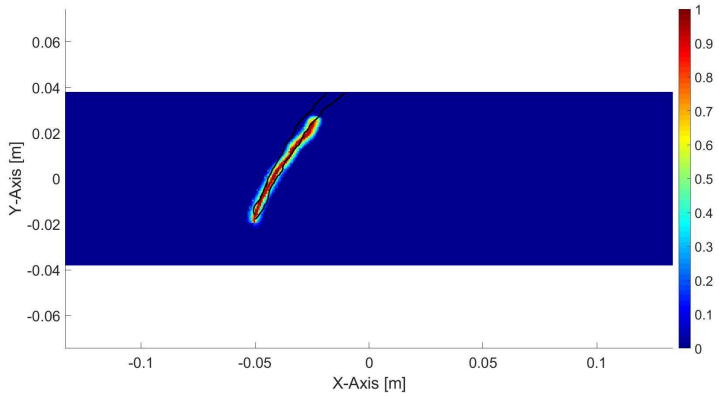

Fig. 16. Fracture path obtained with the stress-based failure criterion; The black line represents the experimental crack patterns.

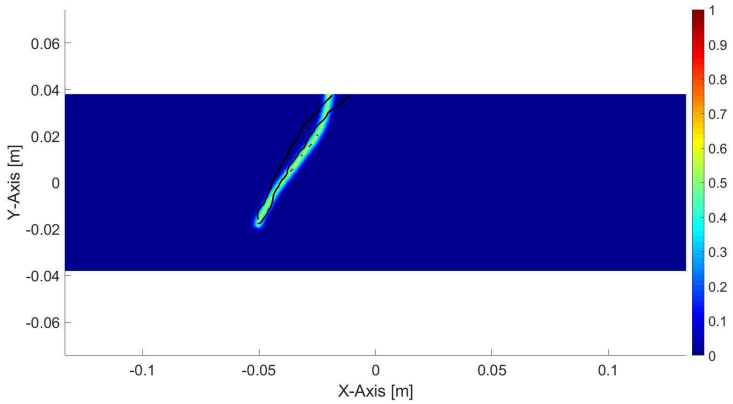

Fig. 17. Fracture path obtained with the critical stretch failure criterion; The black line represents the experimental crack patterns.

5. Conclusion

A novel failure criterion based on the stress field has been proposed in this study for predicting the dynamic crack propagation in brittle materials under mixed-mode I-II loading conditions. The proposed criterion is simple to be implemented numerically and allows to use the well-known failure criteria developed from the classical local theory of mechanics in the framework of ordinary state-based peridynamic theory. The results obtained by analyzing the benchmark problems carried out in this work show how the crack predicted by this approach is in good agreement with the experimental results, especially for mixed-mode loading conditions. Indeed, the approach is capable to capture the onset fracture slope of the growing crack and consequently, the final crack path observed experimentally. Moreover, better results are obtained by applying the proposed method with respect to the critical stretch-based commonly adopted in peridynamics.

Author Contributions

D. Dipasquale carried out the project by running the simulations and writing the manuscript; G. Sarego wrote in-house codes for the implementation of the ordinary state-based peridynamics; P. Prapamonthona, S. Yooyena and A. Shojaei supervised the project. All authors approved the final version of the manuscript.

Acknowledgments

Not applicable.

Conflict of Interest

The authors declared no potential conflicts of interest concerning the research, authorship, and publication of this article.

Funding

This research was financially supported by the International Academy of Aviation Industry, King Mongkut's Institute of Technology Ladkrabang, Bangkok, Thailand. Funded by the Deutsche Forschungsgemeinschaft (DFG, German Research Foundation) – 470246804.

Data Availability Statements

The datasets generated and/or analyzed during the current study are available from the corresponding author on reasonable request.

References

[1] Lal, A., Vaghela, M.B., Mishra, K., Numerical Analysis of an Edge Crack Isotropic Plate with Void/Inclusions under Different Loading by Implementing XFEM, *Journal of Applied and Computational Mechanics*, 7(3), 2021, 1362-1382.
[2] Zhou, S., Rabczuk, T., Zhuang, X., Phase field modeling of quasi-static and dynamic crack propagation: COMSOL implementation and case studies, *Advances in Engineering Software*, 122, 2018, 31-49.
[3] Zhao, J., Modelling of crack growth using a new fracture criteria based peridynamics, *Journal of Applied and Computational Mechanics*, 5, 2019, 498-516.
[4] Belytschko, T., Tabbara, M., Dynamic fracture using element-free Galerkin methods, *International Journal for Numerical Methods in Engineering,* 39(6), 1996, 923-938.
[5] Ortiz, M., Pandolfi, A., Finite-deformation irreversible cohesive elements for three-dimensional crack-propagation analysis, *International Journal for Numerical Methods in Engineering*, 44(9), 1999, 1267-1282.
[6] Pandolfi, A., Ortiz, M., An eigenerosion approach to brittle fracture, *International Journal for Numerical Methods in Engineering*, 92(8), 2012, 694-714.
[7] Spatschek, R., Brener, E., Karma, A., Phase field modeling of crack propagation, *Philosophical Magazine,* 91(1), 2011, 75-95.
[8] Eder, M.A., Chen, X., Alternative Integration Approaches in the Weight Function Method for Crack Problems, *Journal of Applied and Computational Mechanics*, 7(3), 2021, 1719-1725.
[9] Shojaei, A., Mudric, T., Zaccariotto, M., Galvanetto, U., A coupled meshless finite point/Peridynamic method for 2D dynamic fracture analysis, *International Journal of Mechanical Sciences*, 119, 2016, 419-431.
[10] Belytschko, T., Chen, H., Xu, J., Zi, G., Dynamic crack propagation based on loss of hyperbolicity and a new discontinuous enrichment, *International Journal for Numerical Methods in Engineering*, 58(12), 2003, 1873-1905.
[11] Mi, Y., Crisfield, M., Davies, G., Hellweg, H., Progressive delamination using interface elements, *Journal of Composite Materials,* 32(14), 1998, 1246-1272.
[12] Muñoz, J.J., Galvanetto, U., Robinson, P., On the numerical simulation of fatigue driven delamination with interface elements, *International Journal of Fatigue*, 28(10), 2006, 1136-1146.
[13] Abrate, S., Ferrero, J.F., Navarro, P., Cohesive zone models and impact damage predictions for composite structures, *Meccanica*, 50(10), 2015, 2587-2620.
[14] Borden, M.J., Verhoosel, C.V., Scott, M.A., Hughes, T.J.R., Landis, C.M., A phase-field description of dynamic brittle fracture, *Computer Methods in Applied Mechanics and Engineering*, 217-220, 2012, 77-95.
[15] Silling S.A., Reformulation of elasticity theory for discontinuities and long-range forces, *Journal of the Mechanics and Physics of Solids*, 48(1), 2000, 175-209.
[16] Silling S.A., Epton, M., Weckner O., Xu, J., Askari, E., Peridynamic states and constitutive modeling, *Journal of Elasticity*, 88(2), 2007, 151-184.
[17] Silling, S.A., Askari, E., A meshfree method based on the peridynamic model of solid mechanics, *Computers & Structures,* 83(17-18), 2005, 1526-1535.
[18] Shojaei, A., Mossaiby, F., Zaccariotto, M., Galvanetto, U., An adaptive multi-grid peridynamic method for dynamic fracture analysis, *International Journal of Mechanical Sciences,* 144, 2018, 600-617.
[19] Song, Y., Liu, R., Li, S., Kang, Z., Zhang, F., Peridynamic modeling and simulation of coupled thermomechanical removal of ice from frozen structures, *Meccanica*, 55(4), 2020, 961-976.
[20] Nguyen, C.T., Oterkus, S., Oterkus, E., An energy-based peridynamic model for fatigue cracking, *Engineering Fracture Mechanics,* 241, 2021, 107373.
[21] Chen, Z., Jafarzadeh, S., Zhao, J., Bobaru, F., A coupled mechano-chemical peridynamic model for pit-to-crack transition in stress-corrosion cracking, *Journal of the Mechanics and Physics of Solids,* 146, 2021, 104-203.
[22] Silling, S.A., Parks, M.L., Kamm, J.R., Weckner, O., Rassaian, M., Modeling shockwaves and impact phenomena with Eulerian peridynamics, *International Journal of Impact Engineering*, 107, 2017, 47-57.
[23] Behzadinasab, M., Foster, J.T., The third Sandia Fracture Challenge: peridynamic blind prediction of ductile fracture characterization in additively manufactured metal, *International Journal of Fracture,* 218(1), 2019, 97-109.
[24] Wang, Y., Zhou, X., Zhang, T., Size effect of thermal shock crack patterns in ceramics: Insights from a nonlocal numerical approach, *Mechanics of Materials*, 137, 2019, 103-133.
[25] Diana, V., Labuz, J.F., Biolzi, L., Simulating fracture in rock using a micropolar peridynamic formulation, *Engineering Fracture Mechanics*, 230, 2020, 106985.
[26] Ongaro, G., Seleson, P., Galvanetto, U., Ni, T., Zaccariotto, M., Overall equilibrium in the coupling of peridynamics and classical continuum mechanics, *Computer Methods in Applied Mechanics and Engineering*, 381, 2021, 113515.
[27] Bazazzadeh, S., Mossaiby, F., Shojaei, A., An adaptive thermo-mechanical peridynamic model for fracture analysis in ceramics, *Engineering Fracture Mechanics*, 223, 2020, 106708.
[28] Oterkus, S., Madenci, E., Peridynamic modeling of fuel pellet cracking, *Engineering Fracture Mechanics*, 176, 2017, 23-37.
[29] Zaccariotto, M., Shojaei, A., Galvanetto, U., *Coupling of CCM and PD in a meshless way*, E. Oterkus, S. Oterkus, E. Madenci, Peridynamic Modeling, Numerical Techniques and Applications, Elsevier, 2021.
[30] Wang, Y., Zhou, X., Xu, X., Numerical simulation of propagation and coalescence of flaws in rock materials under compressive loads using the extended non-ordinary state-based peridynamics, *Engineering Fracture Mechanics*, 163, 2016, 248-273.
[31] Wang, Y., Zhou, X., Wang, Y., Shou, Y., A 3-D conjugated bond-pair-based peridynamic formulation for initiation and propagation of cracks in brittle solids, *International Journal of Solids and Structures*, 134, 2018, 89-115.
[32] Wang, Y., Zhou, X., Shou, Y., The modeling of crack propagation and coalescence in rocks under uniaxial compression using the novel conjugated bond-based peridynamics, *International Journal of Mechanical Sciences*, 128, 2017, 614-643.
[33] Wang, Y.T., Zhou, X.P., Kou, M.M., Three-dimensional numerical study on the failure characteristics of intermittent fissures under compressive-shear load, *Acta Geotechnica*, 14(4), 2019, 1161-1193.
[34] Zhou, X.P., Wang, Y.T., State-of-the-Art Review on the Progressive Failure Characteristics of Geomaterials in Peridynamic Theory, *Journal of Engineering Mechanics*, 147(1), 2021, 03120001.

[35] Askari, E., Bobaru, F., Lehoucq, R., Parks, M., Silling, S., Weckner, O., Peridynamics for multiscale materials modeling, *Journal of Physics: Conference Series*, IOP Publishing, 2008.
[36] Bobaru, F., Hu, W., The meaning, selection, and use of the peridynamic horizon and its relation to crack branching in brittle materials, *International Journal of Fracture*, 176(2), 2012, 215-222.
[37] Shojaei, A., Hermann, A., Seleson, P., Cyron, C.J., Dirichlet absorbing boundary conditions for classical and peridynamic diffusion-type models, *Computational Mechanics*, 66(4), 2020, 773-793.
[38] Foster, J.T., Silling, S.A., Chen, W., An energy based failure criterion for use with peridynamic states, *International Journal for Multiscale Computational Engineering*, 9(6), 2011, 675-688.
[39] Madenci, E., Oterkus, S., Ordinary state-based peridynamics for plastic deformation according to von Mises yield criteria with isotropic hardening, *Journal of the Mechanics and Physics of Solids*, 86, 2016, 192-219.
[40] Warren, T.L., Silling, S.A., Askari, A., Weckner, O., Epton, M.A., Xu, J., A non-ordinary state-based peridynamic method to model solid material deformation and fracture, *International Journal of Solids and Structures*, 46(5), 2009, 1186-1195.
[41] Tupek, M., Rimoli, J., Radovitzky, R., An approach for incorporating classical continuum damage models in state-based peridynamics, *Computer Methods in Applied Mechanics and Engineering*, 263, 2013, 20-26.
[42] Silling, S.A., Lehoucq, R.B., Peridynamic theory of solid mechanics, *Advances in Applied Mechanics*, 44, 2010, 73-168.
[43] Le, Q., Chan, W., Schwartz, J., A two-dimensional ordinary, state-based peridynamic model for linearly elastic solids, *International Journal for Numerical Methods in Engineering*, 98(8), 2014, 547-561.
[44] Bobaru, F., Zhang, G., Why do cracks branch? A peridynamic investigation of dynamic brittle fracture, *International Journal of Fracture*, 196(1-2), 2015, 59-98.
[45] Ha, Y.D., Bobaru, F., Studies of dynamic crack propagation and crack branching with peridynamics, *International Journal of Fracture*, 162(1), 2010, 229-244.
[46] Ren, H., Zhuang, X., Cai, Y., Rabczuk, T., Dual-horizon peridynamics, *International Journal for Numerical Methods in Engineering*, 108, 2016, 1451-1476.
[47] Renb, H., Zhuanga, X., Rabczuk, T., Dual-horizon peridynamics: A stable solution to varying horizons, *Computer Methods in Applied Mechanics and Engineering*, 318, 2017, 762–782.
[48] Rabczuk, T., Belytschko, T., Cracking particles: a simplified meshfree method for arbitrary evolving cracks, *International Journal for Numerical Methods in Engineering*, 61, 2004, 2316–2343
[49] Ayatollahi, M., Aliha, M., Analysis of a new specimen for mixed mode fracture tests on brittle materials, *Engineering Fracture Mechanics*, 76(11), 2009, 1563-1573.
[50] Dipasquale, D., Sarego, G., Zaccariotto, M., Galvanetto, U., A discussion on failure criteria for ordinary state-based peridynamics, *Engineering Fracture Mechanics*, 186, 2017, 378-398.
[51] Madenci, E., Oterkus, E., *Peridynamic theory, Peridynamic Theory and Its Applications*, Springer, 2014.
[52] Dipasquale, D., Sarego, G., Zaccariotto, M., Galvanetto, U., Dependence of crack paths on the orientation of regular 2D peridynamic grids, *Engineering Fracture Mechanics*, 160, 2016, 248-263.
[53] Nishioka, T., Tokudome, H., Kinoshita, M., Dynamic fracture-path prediction in impact fracture phenomena using moving finite element method based on Delaunay automatic mesh generation, *International Journal of Solids and Structures*, 38(30-31), 2001, 5273-5301.
[54] Ooi, E., Shi, M., Song, C., Tin-Loi, F., Yang, Z., Dynamic crack propagation simulation with scaled boundary polygon elements and automatic remeshing technique, *Engineering Fracture Mechanics*, 106, 2013, 1-21.
[55] John, R., Shah, S.P., Mixed-mode fracture of concrete subjected to impact loading, *Journal of Structural Engineering*, 116, 1990, 585-602.
[56] Ren, B., Wu, C.T., Askari, E., A 3D discontinuous Galerkin finite element method with the bond-based peridynamics model for dynamic brittle failure analysis, *International Journal of Impact Engineering*, 99, 2017, 14-25.

ORCID iD

Daniele Dipasquale https://orcid.org/0000-0003-3479-9861
Giulia Sarego https://orcid.org/0000-0001-9101-5440
Prasert Prapamonthon https://orcid.org/0000-0002-7309-2466
Soemsak Yooyen https://orcid.org/0000-0002-5355-0415
Arman Shojaei https://orcid.org/0000-0001-8638-8285

How to cite this article: Dipasquale D., Sarego G., Prapamonthon P., Yooyen S., Shojaei A. A Stress Tensor-based Failure Criterion for Ordinary State-based Peridynamic Models, *J. Appl. Comput. Mech.*, 8(2), 2022, 617–628.
https://doi.org/10.22055/JACM.2021.38664.3264